

THE PENNSYLVANIA STATE UNIVERSITY
SCHREYER HONORS COLLEGE

DEPARTMENT OF BIOLOGY

THE EFFECT OF SUBCELLULAR ARCHITECTURE ON OSTEOGENIC
DIFFERENTIATION

ANASTASIA MARGARET HALE
SPRING 2020

A thesis
submitted in partial fulfillment
of the requirements
for a baccalaureate degree
in Biology
with honors in Biology

Reviewed and approved* by the following:

Justin Brown
Associate Professor of Biomedical Engineering
Coordinator of the Undergraduate Program
Thesis Supervisor

Daniel Cosgrove
Professor of Biology
Honors Adviser

*** Electronic approvals are on file.**

ABSTRACT

YAP1 is a transcription factor that has been found to localize in the nucleus of subconfluent cells and also has known roles in the Hippo pathway, which controls the growth of organs and suppresses tumor formation through the regulation of cellular proliferation. Recently, studies have investigated the function of YAP1 in osteogenesis, showing that a nanofiber surface can influence the cell signaling pathway and the localization of transcription factors, such as YAP1, specifically through the FAK/RhoA pathway. In order to investigate this phenomenon, I seeded human mesenchymal stem cells (hMSCs) on both electrospun nanofibers and flat PMMA coated surfaces. I used immunofluorescence to quantify relative YAP1 localization in the nucleus and cytoplasm, the number of focal adhesions (measured through vinculin), and FAK phosphorylation. I also stained the actin cytoskeleton and the nucleus in order to measure cell area, circularity, and symmetry. Additionally, I quantified alkaline phosphatase (ALP) to measure relative levels of osteogenic differentiation. Results show that nanofibrous architecture increases nuclear YAP1 localization and focal adhesion size compared to control flat surfaces. Additionally, the nanofiber surface promotes growth of cells with a decreased area and increased symmetry. Cells grown on nanofibrous surfaces also show greater expression of ALP, a marker of osteogenic differentiation. Ultimately, it can be concluded that nanofiber surfaces as compared to flat controls promote osteogenic differentiation through the FAK/RhoA/YAP1 pathway due to increased nuclear localization of YAP1, greater focal adhesion size, and enhanced expression of ALP in cells grown on nanofibrous materials. Understanding the FAK/RhoA/YAP1 pathway through modification of substrate architecture may aid in the development and optimization of biomaterials for tissue regeneration.

TABLE OF CONTENTS

LIST OF FIGURES	iii
LIST OF TABLES	iv
ACKNOWLEDGEMENTS	v
Chapter 1 Introduction	7
Relevance	7
Principles of Bone Regeneration	8
Current Bone Grafting Approaches	9
Role of YAP1 in Osteogenesis	12
Considering the Role of the FAK/RhoA/YAP1 Pathway in Scaffold Design.....	15
Chapter 2 Methods	18
Cell Culture	18
Coverslip Preparation.....	19
Electrospinning of Nanofibers	20
Immunofluorescence Staining	20
Alkaline Phosphatase Detection	21
In- Cell Western Blot.....	22
Statistical Analysis.....	22
Chapter 3 Results	23
Cell Density Experiment.....	23
Nanofiber Experiment.....	25
Experiment 1 – Cell Morphologies and YAP Localization on 10% PMMA Nanofibers	26
Experiment 2 – Cell Morphologies and Focal Adhesion Area on 10% PMMA	
Nanofibers	29
Experiment 3 – Nuclear YAP1 Localization on Small, Medium, and Large Fibers	32
ALP Experiments.....	33
In Cell Western Experiments.....	34
Chapter 4.....	36
Discussion / Future Work	36
Appendix A Supplemental Information.....	38
BIBLIOGRAPHY.....	39

LIST OF FIGURES

Figure 1: Schematic representation of the canonical and non-canonical Hippo signaling pathways. Source: (Low et al., 2014).....	13
Figure 2: Schematic of nanofiber regulation of stem cell osteogenesis via FAK/RhoA/YAP1 Pathway. Source: Chang et al., 2018	15
Figure 3: Signaling proteins associated with FAK. Source: Schlaepfer at al., 1999.....	16
Figure 4: Average proportion of YAP1-negative nuclei in mMSCs fixed at 1-, 3-, and 7-day time points. * indicates $p < 0.05$ compared with 24-hour time point.	23
Figure 5: YAP1 fluorescence (green) and nuclei (purple) in mMSCs fixed at 24 hours	24
Figure 6: YAP1 fluorescence (green) and nuclei (purple) in mMSCs fixed at 72 hours	24
Figure 7: YAP1 fluorescence (green) and nuclei (purple) in mMSCs fixed at 1 week.....	24
Figure 8: 3% PMMA Nanofibers	25
Figure 9: 6.5% PMMA Nanofibers.....	25
Figure 10: 10% PMMA Nanofibers	25
Figure 11: Average cell area of hMSCs seeded on 10% PMMA nanofibers or a PMMA control flat surface. *indicates $p < 0.05$ compared to control.	26
Figure 12: Average cell circularity of hMSCs seeded on 10% PMMA nanofibers or a PMMA control flat surface. * indicates $p < 0.05$ compared to control.....	26
Figure 13: Average cell symmetry of hMSCs seeded on 10% PMMA nanofibers or a PMMA control flat surface. * indicates $p < 0.05$ compared to control.....	27
Figure 14: Average cell symmetry of hMSCs seeded on 10% PMMA nanofibers or a PMMA control flat surface. * indicates $p < 0.05$ compared to control.....	27
Figure 15: YAP staining (pink) of hMSC on PMMA control surface	28
Figure 16: YAP staining (pink) of hMSC on 10% PMMA Nanofiber.....	28
Figure 17: Average cell area of hMSCs seeded on 10% PMMA nanofibers or a PMMA control flat surface. * indicates $p < 0.05$ compared to control.	29
Figure 18: Average cell circularity of hMSCs seeded on 10% PMMA nanofibers or a PMMA control flat surface. * indicates $p < 0.05$ compared to control.....	29
Figure 19: Average cell symmetry of hMSCs seeded on 10% PMMA nanofibers or a PMMA control flat surface. * indicates $p < 0.05$ compared to control.....	30

Figure 20: Average focal adhesion area of hMSCs seeded on 10% PMMA nanofibers or a PMMA control flat surface.	30
Figure 21: Vinculin staining (green) of hMSC on PMMA control surface.....	31
Figure 22: Vinculin staining (green) of hMSC on 10% PMMA Nanofiber	31
Figure 23: Average nuclear YAP1 fluorescence intensity of hMSCs seeded on 3%, 6.5%, or 10% nanofibers or a PMMA control flat surface. * indicates $p < 0.05$ compared to control. ** indicates $p < 0.05$ compared to 3% nanofibers.....	32
Figure 24: ALP activity of hMSCs seeded on 7.5% PMMA nanofibers or a PMMA control flat surface and incubated for 48 hours. * indicates $p < 0.05$ compared to control	33
Figure 25: Average integrated FAK576 intensity of hMSCs seeded on 7.5% PMMA nanofibers or a PMMA control flat surface as indicated by in-cell western blot. n=2.	34

LIST OF TABLES

Table 1: Average Proportion of YAP1 Negative Nuclei at Different Time Points	38
Table 2: P-Values for Time Course Experiment	38
Table 3: Average Area, Aspect Ratio, Circularity Index, and Nuclear YAP1 Intensity of hMSCs seeded on 10% PMMA Nanofibers and Control Surfaces.....	38
Table 4: P-Values for Nanofiber Experiment 1	38
Table 5: Average Area, Aspect Ratio, Circularity Index, and Vinculin Patch Area of hMSCs seeded on 10% PMMA Nanofibers and Control Surfaces.....	39
Table 6: P-Values for Nanofiber Experiment 2	39
Table 7: Average Nuclear YAP1 Intensity of hMSCs seeded on 3,6.5, or 10% PMMA Nanofibers or a Flat Control Surface.....	39
Table 8: P-Values for Nanofiber Experiment 3	39
Table 9: Average ALP Intensity of hMSCs grown on 7.5% PMMA Nanofibers or Flat Control Surfaces.....	40
Table 10: Average Intensity of FAK576 of hMSCs Seeded on 7.5% PMMA Nanofibers of Flat Control Surfaces.....	40

ACKNOWLEDGEMENTS

I would like to thank Dr. Brown and all the graduate students who have helped me along the way, specifically Dan, Brittany, Pouria, and Merve. Thank you for being patient with me and teaching me so much during these past 4 years.

Additionally, thank you to the best lab partner, Coreena Chan. I would not have been able to do this without you. Some of my favorite memories include eating takeout in the hallway together while we waited hours for things to work. Being in lab without you there this past year was not the same!

Chapter 1

Introduction

Relevance

The worldwide phenomenon of bone injury has been rapidly increasing and continues to rise due to factors such as high rates of obesity, lack of physical activity, and an aging population (1). Current treatment involves bone autographs or allografts which are used in approximately 2.2 million orthopedic procedures annually. However, the usage of these grafts is limited by donor-site morbidity and supply (2). For example, autologous bone graft involves comorbidity associated with the presence of a donor site. This procedure has been shown to result in chronic pain in a range of 2.5% from 8% of cases, dysesthesia in 6% of cases, or infection in 2% of cases. Some of these procedures also require anesthesia that would not otherwise be needed if an autograph was not involved, increasing the surgical risks for the patient. Moreover, the use of allogenic bone involves additional risks, including the possibility of disease transmission. Allogenic bone usage is also expensive due to necessary treatment and sterilization of the specimen before implantation (3). Ultimately these factors contribute to the need for a non-patient derived clinically available bone substitute for surgical use.

In recent years, efforts have been made to engineer bone tissue that can be placed in the human body. Approaches include three-dimensional, porous, degradable, polymeric scaffolds which allow the ingrowth of new tissue as well as cells cultured on preformed three-dimensional scaffolds which can then be transplanted directly into the patient (4). While these scaffolds are

promising methods of stimulating bone growth, their architectures must be evaluated for the optimization of cellular attachment, migration, proliferation and differentiation (5).

Principles of Bone Regeneration

Bone regeneration is a complex, well-arranged and regulated process that continues as bone remodeling throughout adult life. One of the major applications of bone regeneration in the body is observed during fracture healing (5). During fracture healing, the bone heals itself so that it can continue to transfer mechanical loads. Ultimately, the bone is regenerated, and the properties of the preexisting tissue largely are restored through four responses including those of the bone marrow, cortex, periosteum, and external soft tissues (6).

The responses of fracture healing have been broken down into two additional categories: primary fracture healing which includes the bone marrow and cortex, and secondary formation which involves the formation of a callous through the periosteum and soft tissues (6). Initially after bone injury, bleeding occurs between the damaged bone ends and a clot is formed between the fragments. Mast cells and other inflammatory elements appear and begin to clear away the debris, and increased cell division begins in the periosteum and surrounding tissue. A fracture blood clot forms between the two damaged ends of bone and is invaded by fibrovascular tissue which eventually replaces the clot and lays down the foundation of the matrix of the primary callous. The surrounding soft tissues also help to develop an extraosseous blood supply which serves to supply the forming callous. The callous is then removed and replaced with normal bone through the function and recruitment of osteoclasts and osteoblasts (7). While most fractures heal

on their own without the formation of scar tissue, there are still some cases where the bone regeneration is impaired and grafting techniques must be used to fully heal the bone (5).

Current Bone Grafting Approaches

There are currently a wide array of clinical approaches to repair damaged bone that will not heal on its own. These techniques include distraction osteogenesis, bone transport, and a number of bone grafting methods. Distraction osteogenesis and bone transport both involve the induction of bone regeneration through gradually distracted osseous surfaces. For example, an external fixator or an intramedullary lengthening device may be connected between the two bone segments in order to stimulate bone growth. However, these methods induce bone growth very slowly, around 1 mm per day, and are very technically demanding (5).

Bone grafting can also be used to repair bone, and a number of techniques such as autologous bone grafts, allografts, and bone-graft substitutes have been developed, all with unique sets of benefits and limitations. Autologous bone grafting is currently regarded as the most effective method, and it involves the harvesting of bone from one's own body, most commonly the anterior and posterior iliac crests of the pelvis or intramedullary canal of long bones. Because the bone is from the patient's own body, it is histocompatible and non-immunogenic, reducing the probability of infection and rejection. However, the harvesting requires an additional surgery for the patient and is limited to how much bone can be harvested safely. Allogenic bone grafting is a relatively similar procedure but involves the harvesting of bone from a cadaver or external source. This of course involves the potential for rejection or disease transmission as well as limits to harvest quantity and availability. Finally, bone-graft

substitutes such as scaffolds which are created to promote the migration, proliferation and differentiation of bone cells can be used. Current examples include collagen, hydroxyapatite (HA), β -tricalcium phosphate (β -TCP) and calcium-phosphate cements, and glass ceramics. While these scaffolds are promising for the regeneration of large quantities of bone without the limitations of donor morbidity and supply, they do not have the same biological or mechanical properties as bone (5). The goal is to eventually develop a bone scaffold with cells that can recapitulate the function and structure of bone in the human body.

Nanofiber Surfaces to Guide Cell Behavior

In order to create an effective scaffold that successfully recapitulates bone growth in vivo, it is important to understand the mechanisms of cell behavior and migration. Cell migration is significant in humans from conception to death, as the forming embryo is guided by specific cells and factors that allow for its proper functional development. For example, during gastrulation the embryo becomes tri-layered through calculated movement of large groups of cells. Moreover, cell migration is a vital component of tissue regeneration and repair as immune cells migrate to centers of damage to rid the body of unwanted debris (8).

Another vital component of cellular migration are integrins and the formation of focal adhesions. For migration to occur, a protrusion must become established and stabilize itself by attaching to surrounding elements. Integrins function as receptors and support adhesion of the cell to the extracellular matrix (ECM) or to surrounding cells by making connections with actin filaments located inside the cell. This allows the signaling inside of the cell to interact and detect its outside environment. Focal adhesion formation is also vital to the successful migration of cells; however, little is known about their role in response to the extracellular environment (8).

These concepts apply to an important facet of tissue engineering known as mechanosensing. Studies have shown that migration and the cytoskeletal mechanics of cells, including focal adhesion formation, are modulated both by the stiffness and deformation energy of the substrate they are grown on. These physical cues between the cell and its physical environment are vital for the control of cell mechanics. Specifically, the ability of the cell to generate force through the actin cytoskeleton, the site of force transmission, and the intracellular environment of where the application of force originates (9).

Moreover, the extracellular matrix is composed of organized fibers such as fibronectin and collagen. It has been proposed that creating a fibrous structure that mimics the ECM is vital to promote the growth and differentiation of cells that will be used to create tissue scaffolds (10). Various studies have shown that nanofiber scaffolds promote proliferation, adhesion, and differentiation of cells (11,12). Additionally, it has been revealed that a nanofibrous architecture increases cellular stiffness and promotes mechanotransduction through Myosin IIA and ROCK II activity (10). More recently, a study showed that nanofibers regulate osteogenesis through the FAK/RhoA/YAP1 pathway (13). Ultimately, in order to create the most effective scaffolds it is vital to continue the study of cell-cell and cell-ECM interactions and through which mechanisms cells translate these topographical cues, particularly as they are related to nanofibrous architecture.

Role of YAP1 in Osteogenesis

Of late, studies have investigated the function of YAP1 in osteogenesis, showing that a nanofiber surface can influence the cell signaling pathway and the localization of transcription factors, such as YAP1, specifically through the FAK/RhoA pathway (13). YAP1 is a mechanosensitive transcriptional regulator that has roles in controlling cellular proliferation and suppressing genes that promote apoptosis (14). YAP1 is also involved in many important cell signaling pathways such as the Hippo pathway, which regulates organ growth and the MAP Kinase/ERK pathway which is involved in the regulation of cell cycle progression (15).

The Hippo pathway is primarily composed of two kinases, MST and LATS which control the activity of the transcriptional co-activators YAP and TAZ. When MST and LATS respond to upstream stimuli, the MST-activated LATS kinase phosphorylates YAP and TAZ at a specific Serine residue located in the amino-terminal region of each protein. Shortly after, the 14-3-3 proteins recognize a specific motif surrounding the LATS-phosphorylated Serine, allowing for strong protein-protein interactions to be established. This complex then forces YAP and TAZ into the cytoplasm rather than the nucleus. However, if the LATS-kinase is inhibited, then YAP and TAZ are permitted to enter the cell nucleus and drive proliferation through transcriptional regulation (16).

The Hippo pathway is regulated by a variety of factors including, G protein-coupled receptors (GPCRs), LIF receptors, E-cadherins, and adherens junctions. YAP can also be directly regulated by LATS-kinase, otherwise known as canonical signaling.

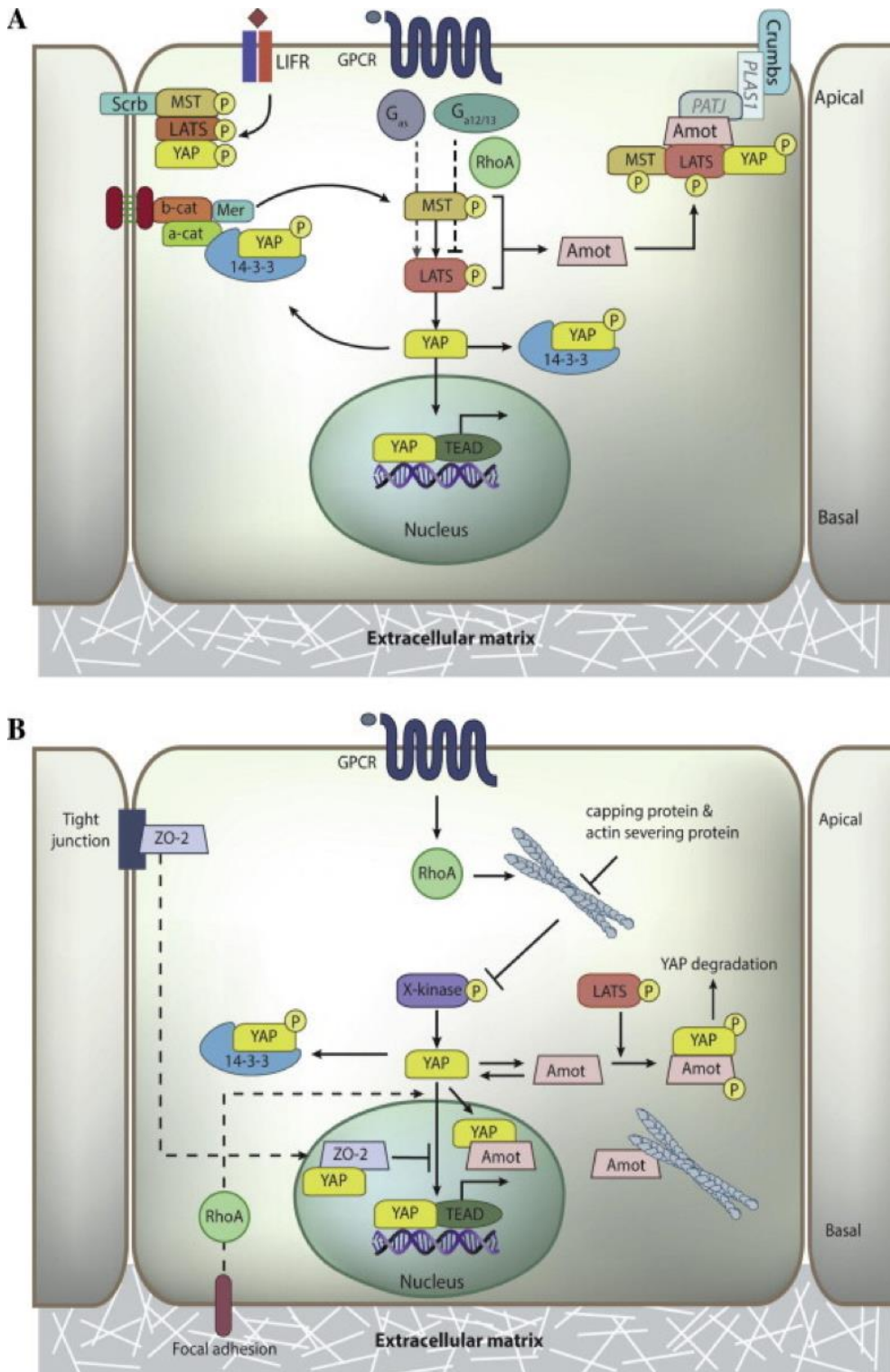


Figure 1: Schematic representation of the canonical and non-canonical Hippo signaling pathways. Source: (Low et al., 2014)

More importantly however, YAP and TAZ activity have been found to be regulated by the microenvironment through physical and mechanical cues. For example, a study has shown that YAP/TAZ become localized to the nucleus on hard surfaces but remain cytoplasmic on soft substrates. Additionally, YAP/TAZ are primarily regulated by cell spreading in the ECM, and cytoskeletal tension is necessary for their nuclear localization. This study found that not only are YAP/TAZ required for cellular differentiation as mediated by ECM stiffness and cellular geometry, but they can also change the behavior of cells grown on soft matrices, or those not conducive to cellular differentiation and proliferation (17). Interestingly, this regulation was found to be independent of LATS phosphorylation downstream in the Hippo cascade.

YAP/TAZ activity can also be modulated by a number of alternative pathways. For example, it has been shown that inhibition of RhoA, an activator of F-actin contraction, plays a role in increasing the phosphorylation of YAP/TAZ independent of LATS (16). Moreover, actomyosin contractility has been shown to suppresses YAP phosphorylation at Ser¹¹². However, in the absence of cell-cell contact and contractility, Ser¹¹² phosphoregulation was quashed by actin cytoskeletal integrity leading to nuclear localization of both phospho- and non-phospho-YAP. These data suggest potential regulation of YAP through two mechanisms, actomyosin contractility and cytoskeletal integrity (18). Understanding how these pathways work together or function in relation to one another to regulate YAP/TAZ localization and activity is crucial for designing scaffolds with optimal cell migration and differentiation capabilities.

Considering the Role of the FAK/RhoA/YAP1 Pathway in Scaffold Design

Recently, a mechanistic study revealed that nanofibers regulate osteogenesis of bone marrow stem cells through the FAK/RhoA/YAP1 pathway (13).

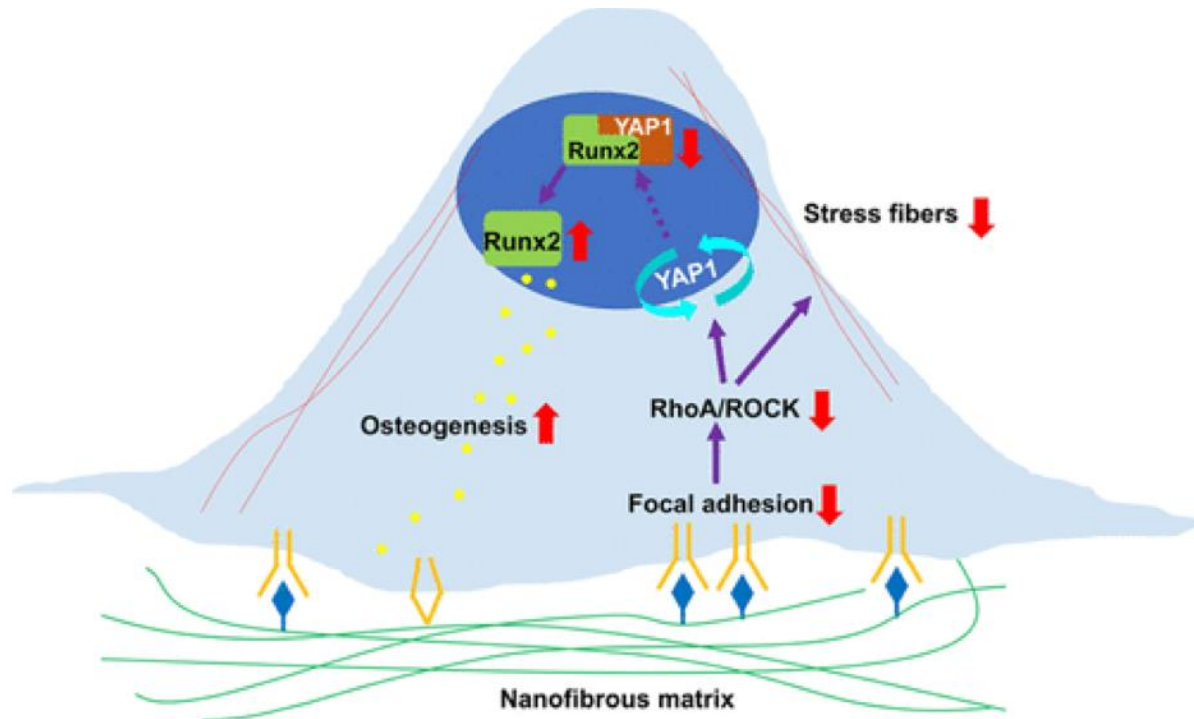


Figure 2: Schematic of nanofiber regulation of stem cell osteogenesis via FAK/RhoA/YAP1 Pathway.
Source: Chang et al., 2018

Focal Adhesion Kinase (FAK) is an important cellular adhesion protein that plays a role in linking integrin receptors with a variety of intracellular signaling pathways and colocalizing with these integrin receptors at anchorage sites to form focal adhesions (19). FAK localizes to these sites through C-terminal-domain-mediated interactions with integrin-associated proteins such as paxillin and talin. Additionally, FAK becomes phosphorylated at 7 to 8 different sites after engaging with integrin matrix proteins. FAK functions as part of cytoskeleton-associated network of signaling proteins which act to convert signals generated from integrins to mitogen-

activated protein (MAP) kinase cascades and is essential for integrin-stimulated cell migration. FAK also associates with activated growth-factor receptors through its N-terminal domain and has an important function in promoting PDGF- and EGF-stimulated cell migration (20).

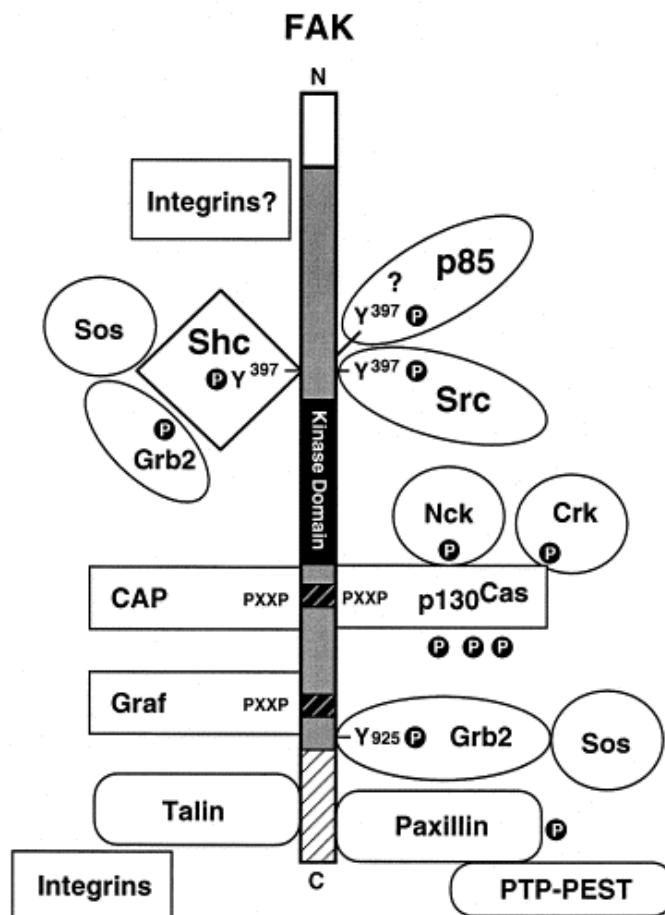


Figure 3: Signaling proteins associated with FAK. Source: Schlaepfer et al., 1999

RhoA is a small GTPase that has been shown to affect cellular lineage commitment and differentiation as well as YAP/TAZ nuclear localization by promoting the formation of actin bundles and stress fibers in response to cell spreading across the ECM. RhoA is a part of the Rho GTPase pathway which is required to foster the maturation of FAs in cells in contact with the

ECM and modulate YAP transcriptional activity (21). RhoA also in turn activates ROCK which is responsible for formation of stress fibers and focal adhesions, activation of Myosin II, and stabilization of cortical actin (22).

Ultimately, polymerization of the cytoskeleton, specifically due to mechanical cues, leads to FAK and RhoA signaling which transmit signals to regulate gene expression through activity of YAP1 (23). Further understanding of the FAK/RhoA/YAP1 pathway is crucial for enhanced design of nanofibrous scaffolds and the advancement of tissue engineering, especially as it relates to osteogenesis.

Chapter 2

Methods

Cell Culture

Mouse or human mesenchymal stem cells were obtained and cultured in alpha-modified minimum essential medium (α -MEM) with 10% fetal bovine serum (FBS), and 1% penicillin/streptomycin (Pen/Strep). Cells were cultured in a humidified incubator at 37°C and 5% CO₂. Cells were rinsed with 10X Phosphate Buffered Saline (PBS) which was prepared with deionized water containing 1.35 M NaCl, 7mM KCl, 16 mM NA₂HPO₄•7H₂O, and 18 mM KH₂PO₄. The pH was adjusted to 7.4 using NaOH and HCl, and the solution was then filtered with a funnel.

When cells reached 80% confluency, they were passed to either a larger plate to continue to grow or seeded into a 6-well plate for further experimentation. Media was aspirated from the dish, and about 5-7 mL of PBS were added to the dish depending on the size. The PBS was aspirated, and about 2 mL of Trypsin was added to the dish. Cells were placed in the incubator for 5 minutes, and then the plates were tapped on the sides to ensure removal of all cells from the surface. 10 mL of media was then added to the trypsin fraction and then cells were centrifuged for 5 minutes at 300g. The excess media was aspirated, and the pellet was resuspended in 10 mL of new media. From there the cells were either directly placed into a new dish or counted with a hemacytometer. Once counted, the cells would be seeded in a 6-well plate on top of a coverslip either coated in PMMA or with a PMMA nanofiber surface. Cells were seeded at a density of 10,000 cells/cm².

To freeze cells, cells were resuspended after centrifuging in a media containing 60% regular media, 20% FBS, and 20% DMSO. The same amount of regular media was then added to this mixture, and 1.5 mL of the total cell suspension was then added to individual cryo vials which were labeled with the date, cell type, and passage number. The vials were placed in a special container containing isopropyl alcohol for 24 hours at 80°C . After 24 hours, the cells were placed in a liquid nitrogen tank for storage until they were to be thawed.

To thaw cells, a vial was removed from the liquid nitrogen stock and placed in a warm water bath until only a small block of ice remained. The cells were added to a 10 mL falcon tube, and 10 mL of media was slowly added dropwise on top. The solution was centrifuged for 5 min at 300g, the remaining media was aspirated, and the cells were resuspended in 10 mL of fresh media and placed in a 10 cm dish. Each vial contains about 1×10^6 cells.

Coverslip Preparation

To prepare for spin coating, glass coverslips were soaked overnight in KOH diluted in deionized H_2O . The coverslips were then washed in isopropanol for 5 minutes, quickly rinsed with DI H_2O , and carefully dried around the edges with a Kim wipe. The slides were placed one by one on a spin coater where they were covered in 100 μL of 4% Poly-methyl methacrylate (PMMA) diluted in nitromethane and spun at 5000 rpm for 10 seconds.

Electrospinning of Nanofibers

PMMA nanofibrous substrates were prepared using an electrospinning box with a syringe pump and a highly conductive copper target. PMMA was dissolved in a 3:1 dimethylformamide:tetrahydrofuran solution and loaded into a 1 mL syringe with a needle at its tip. 10 kV of voltage was applied between the tip of the needle and the copper target with a flow rate of 6 mL/hr. The fibers were collected on glass coverslips which were attached to the copper surface about 15-18 cm away from the tip of the needle. The coverslips were previously spin coated in 2% poly (2-hydroxyethyl methacrylate) (PHEMA) dissolved in 70% ethanol at 5000 rpm for 10 seconds using the technique as previously described. PHEMA was used because it prevents the adhesion of cells to the glass coverslip. The nanofiber covered slides were then heated two times on a hot plate at 120 °C for 1 min each and sterilized with UV treatment in the cell culture hood before experimentation.

Immunofluorescence Staining

To begin immunofluorescence staining of cells, the coverslips were washed once with 1 mL of PBS. Next, 1 mL of cytoskeleton stabilization buffer containing 50 mM NaCl, 0.5% Triton, 10 mM PIPES, 2.5 mM MgCl₂, 1 mM EGTA, protease and phosphatase inhibitors amounting to 100 µL per 10 mL, and adjusted to a pH of 6.8 using NaOH and HCl was added to each slide for 1 minute, and then aspirated. The slides were washed again in PBS. Next, slides were fixed in a solution containing 3.7% formaldehyde (37% paraformaldehyde in 1 x PBS) for 15 minutes. After fixation, slides were rinsed 3 times in 1 x PBS and permeabilized for 45 minutes by a buffer containing 2% Bovine Serum Albumin and 0.1% Triton in 1 x PBS. The

slides were then incubated for an hour at room temperature with either an anti-YAP1 antibody (1:500), anti-vinculin antibody (1:400), anti-integrin beta 5 (1:400), or anti-FAK 576 (1:1000). The cells were washed once again 3 times in PBS and then incubate in the dark for 45 minutes with a secondary antibody corresponding to the primary antibodies used, in most cases either Alexa Fluor goat anti-rabbit (1:400), or anti-mouse (1:250). After aspiration of the secondary solution. slides were rinsed 3 times in 1 x PBS, and slides were incubated with Alexa Fluor phalloidin (1:1500) and DAPI (1:1000) for 30 minutes in the dark. Slides were washed for the last time 3 times in 1 x PBS and mounted to microscope slides with a liquid mounting solution. The coverslips dried overnight in the dark and were then sealed with a thin coating of clear nail polish around the edges.

After staining, the slides were imaged under a Leica Dm 5500B microscope using water immersion at 20x. Approximately 50 images were taken at random per set and the images were run through cell profiler or image j for more detailed analysis.

Alkaline Phosphatase Detection

Mouse or human mesenchymal stem cells were grown on either flat surfaces covered with PMMA or nanofibrous surfaces for 7 days and then lysed with Mammalian Extraction Reagent (M-PER) and subject to one freeze-thaw cycle. The samples were incubated in a p-nitrophenol phosphate solution for 30 minutes and osteogenic differentiation was quantified via absorbance. Data was normalized to fluorescence values obtained from a Pico Green dsDNA Assay, made with a 200-fold dilution starting from a 1 µg/mL stock solution.

In- Cell Western Blot

To begin the in cell western blot, the same procedures were followed as the immunofluorescence protocol, using anti-FAK 576 (1:1000) as a primary antibody and goat-anti rabbit IR 800 dye (1:5000) as a secondary. A cell tag 700 stain was also added in tandem with the secondary antibody (1:500) for 45 minutes in the dark. Additionally, a control well with only the secondary antibody was added to subtract background noise from the results. After the slides were mounted, they were scanned using the Licor Odyssey Machine's in-cell western feature, and the 800 channels were divided by the 700 to obtain relative FAK intensities, normalized to the whole cell fraction.

Statistical Analysis

The quantitative data from the images obtained from the immunofluorescence experiments were analyzed with Cell Profiler and Image J Software, specifically cell area, circularity index, aspect ratio, fluorescence intensity, nuclear area, and focal adhesion size. The data were analyzed with t-test and statistical significance was set at $p < 0.05$. For the nanofiber experiments, nanofiber and control slides were compared to one another using an average of 40-50 slides per experimental condition. Multiple sets of data were produced from singular experiments. Each condition had an n of either 2 or 3 from replicate slides per experiment set.

Chapter 3

Results

Cell Density Experiment

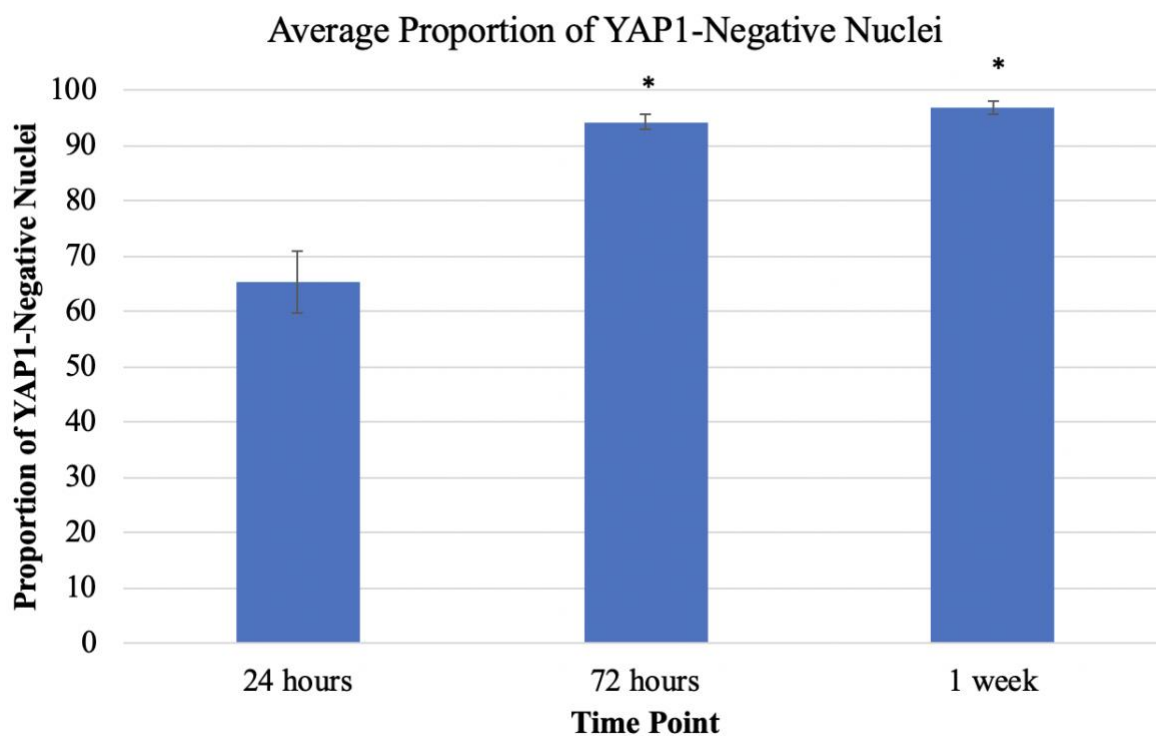


Figure 4: Average proportion of YAP1-negative nuclei in mMSCs fixed at 1-, 3-, and 7-day time points. * indicates $p < 0.05$ compared with 24-hour time point.

In this experiment, mouse MSCs were seeded onto glass coverslips at a density of 10,000 cells / cm² and the cells were fixed at one day, three day, and seven-day time points. The cells were stained for YAP1, and the nuclei were counterstained with DAPI. Representative images of the slides from each time point were taken and the percent of cells with cytoplasmic YAP localization was calculated. In the images, YAP is green, and nuclei are purple, so nuclear YAP localization results in a white color. Cells fixed after one day had an average cytoplasmic YAP

localization of 65.2% and those at day three and day seven were higher with 94.2% and 96.8% cytoplasmic YAP localization, respectively. These results were significant when comparing day one and day three and day one and day seven with $p < 0.05$. Ultimately, these results suggest that greater confluency results in greater cytoplasmic YAP localization.

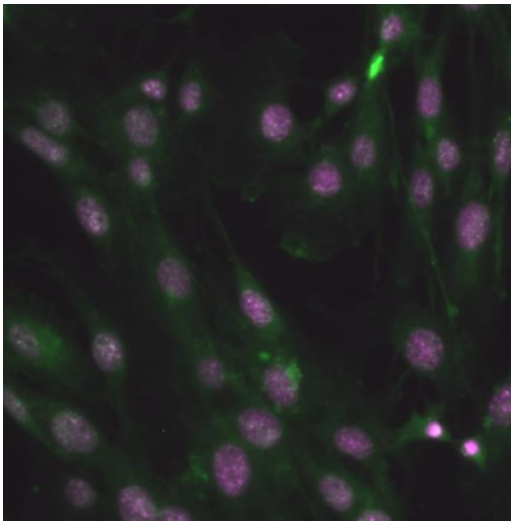


Figure 5: YAP1 fluorescence (green) and nuclei (purple) in mMSCs fixed at 24 hours

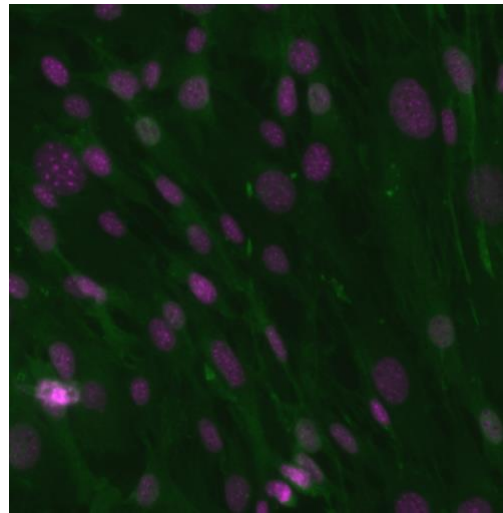


Figure 6: YAP1 fluorescence (green) and nuclei (purple) in mMSCs fixed at 72 hours

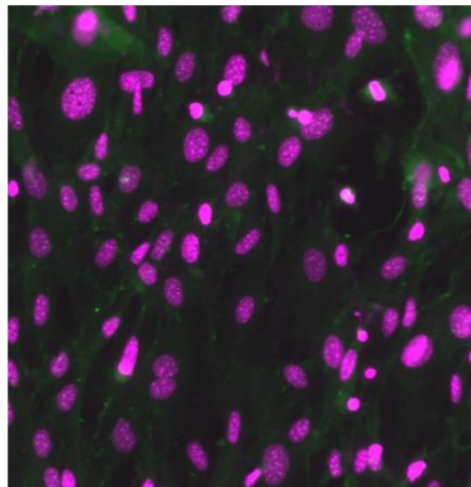


Figure 7: YAP1 fluorescence (green) and nuclei (purple) in mMSCs fixed at 1 week

Nanofiber Experiment

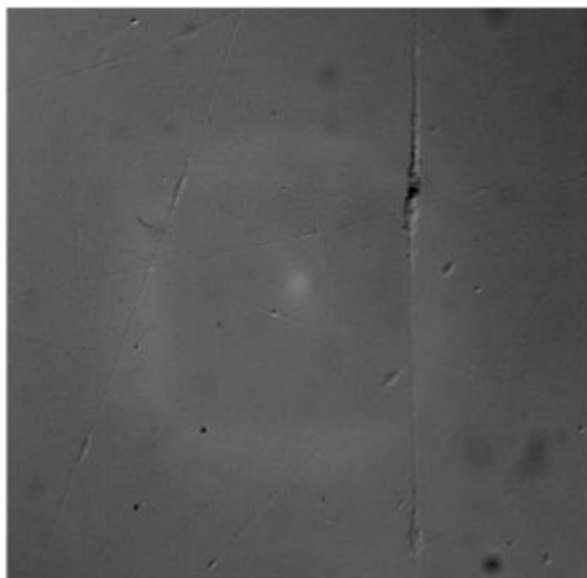


Figure 8: 3% PMMA Nanofibers

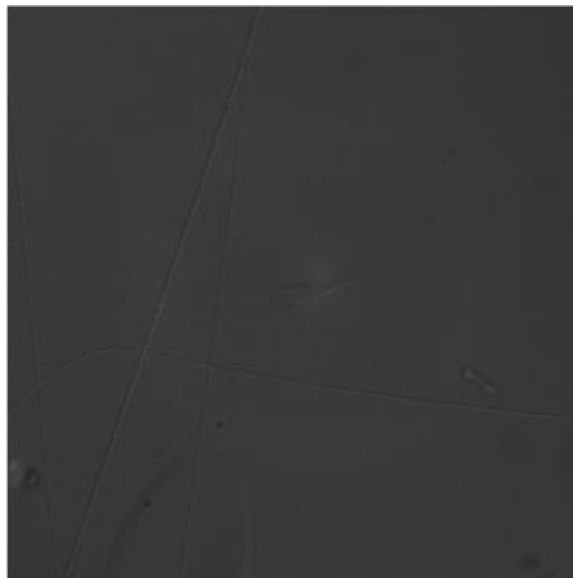


Figure 9: 6.5% PMMA Nanofibers

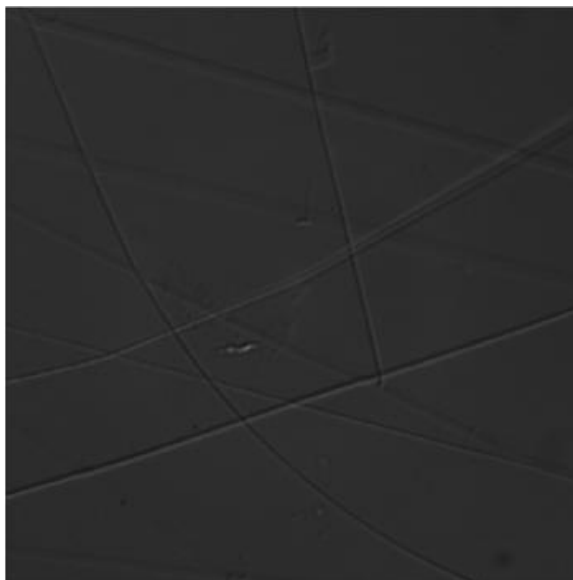


Figure 10: 10% PMMA Nanofibers

Experiment 1 – Cell Morphologies and YAP Localization on 10% PMMA Nanofibers

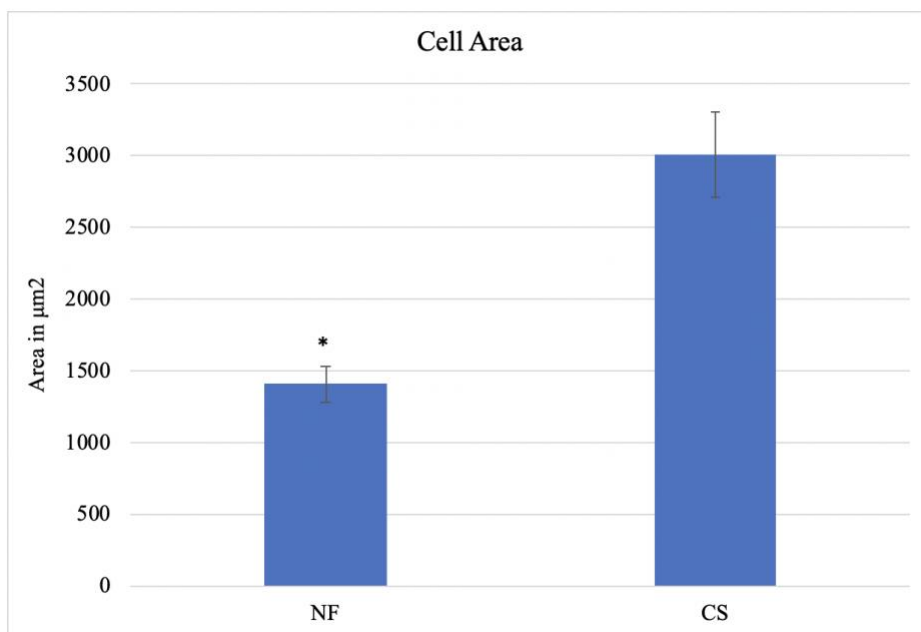


Figure 11: Average cell area of hMSCs seeded on 10% PMMA nanofibers or a PMMA control flat surface. *indicates $p < 0.05$ compared to control.

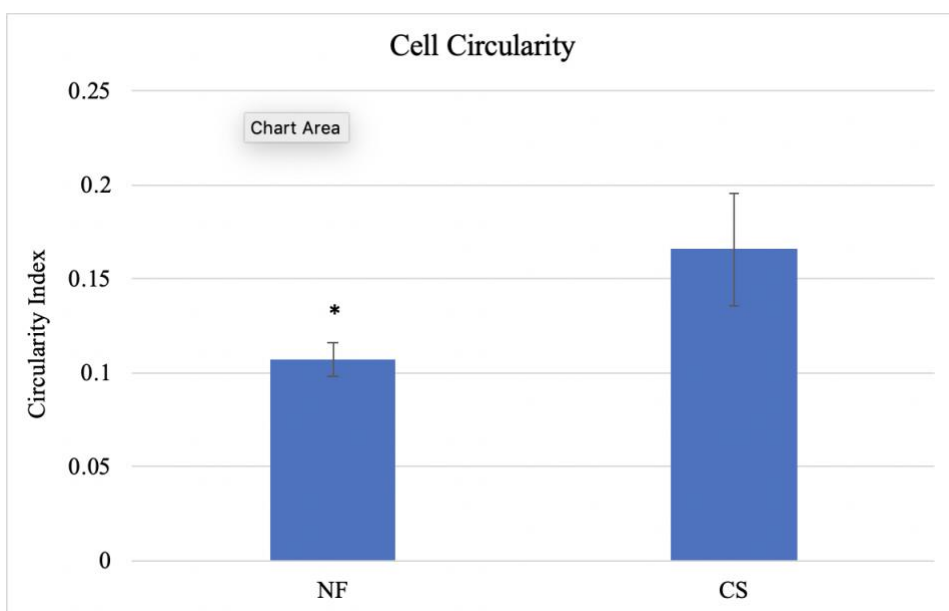


Figure 12: Average cell circularity of hMSCs seeded on 10% PMMA nanofibers or a PMMA control flat surface. * indicates $p < 0.05$ compared to control.

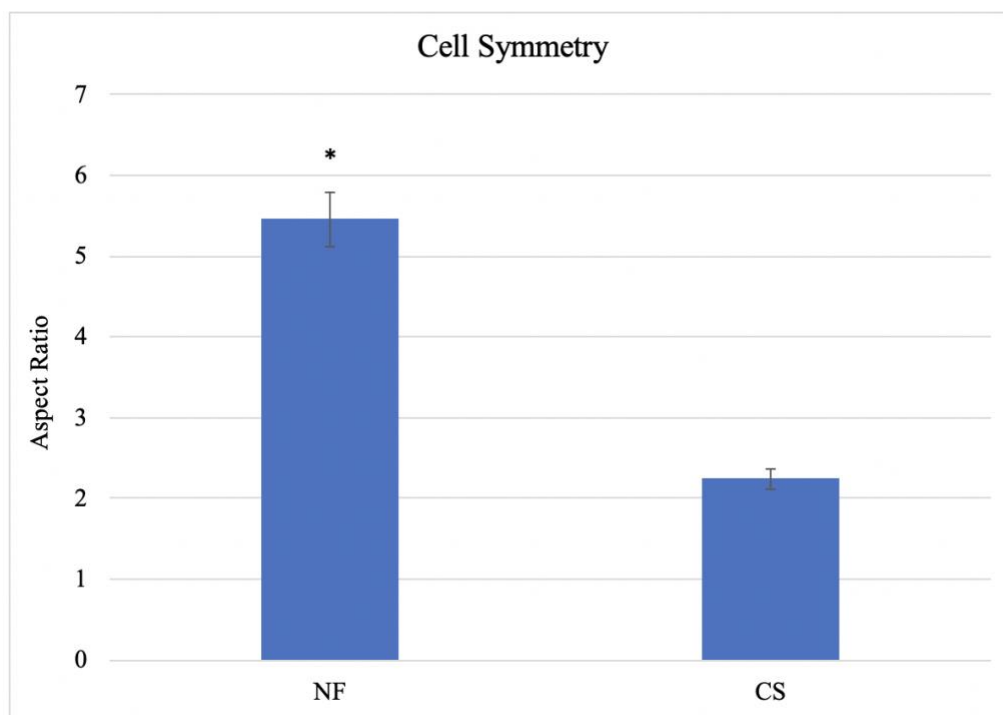


Figure 13: Average cell symmetry of hMSCs seeded on 10% PMMA nanofibers or a PMMA control flat surface. * indicates $p < 0.05$ compared to control.

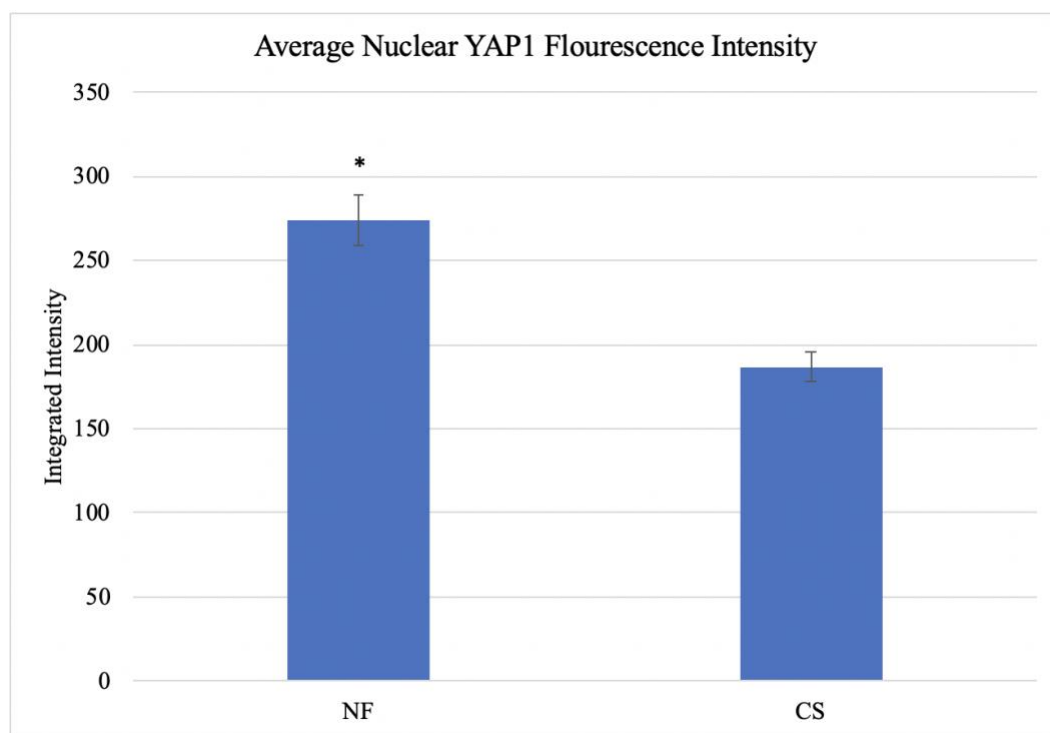


Figure 14: Average cell symmetry of hMSCs seeded on 10% PMMA nanofibers or a PMMA control flat surface. * indicates $p < 0.05$ compared to control.

In this experiment, human MSCs were seeded onto glass coverslips at a density of 5,000 cells / cm². Cells were fixed after 24 hours and stained for YAP, actin, vinculin, and DAPI. Images were taken and plugged into Cell Profiler for data analysis. Cell morphologies of hMSCs were quantified by the circularity index ($CI=4\pi A/L^2$) and aspect ratio (AR), where A is the area of the cell and L is the perimeter. The circularity index is a measure of the circularity of a cell whereas the aspect ratio is a measure of symmetry and is the ratio of the major cell axis length to the minor cell axis length. CI=1 represents a perfect circle and AR=1 represents absolute symmetry. Findings from experiment one showed that hMSCs grown on nanofiber surfaces have a smaller cell area (1407.11 vs 3004.48 μm^2) and circularity (0.11 vs 0.17), but a greater cell symmetry (5.5 vs 2.2) as compared to cells grown on control surfaces. The nanofiber surface also showed an increase in the nuclear localization of YAP as compared to the control (274 vs 186), suggesting that nanofiber surfaces play a role in enhancing the growth of mesenchymal stem cells, promoting osteogenic differentiation.

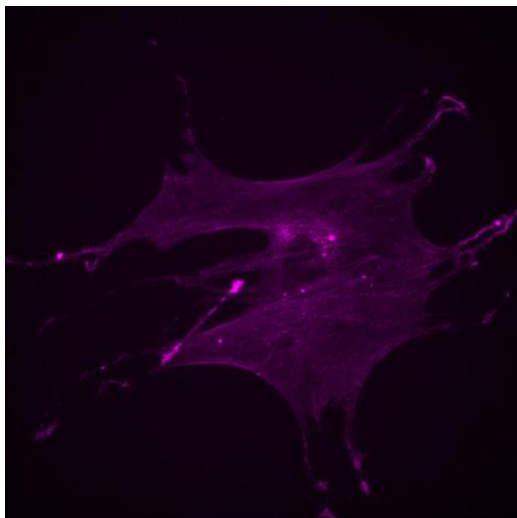


Figure 15: YAP staining (pink) of hMSC on PMMA control surface

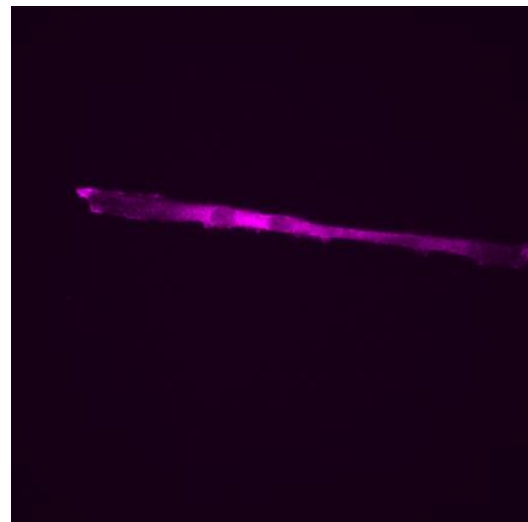


Figure 16: YAP staining (pink) of hMSC on 10% PMMA Nanofiber

Experiment 2 – Cell Morphologies and Focal Adhesion Area on 10% PMMA Nanofibers

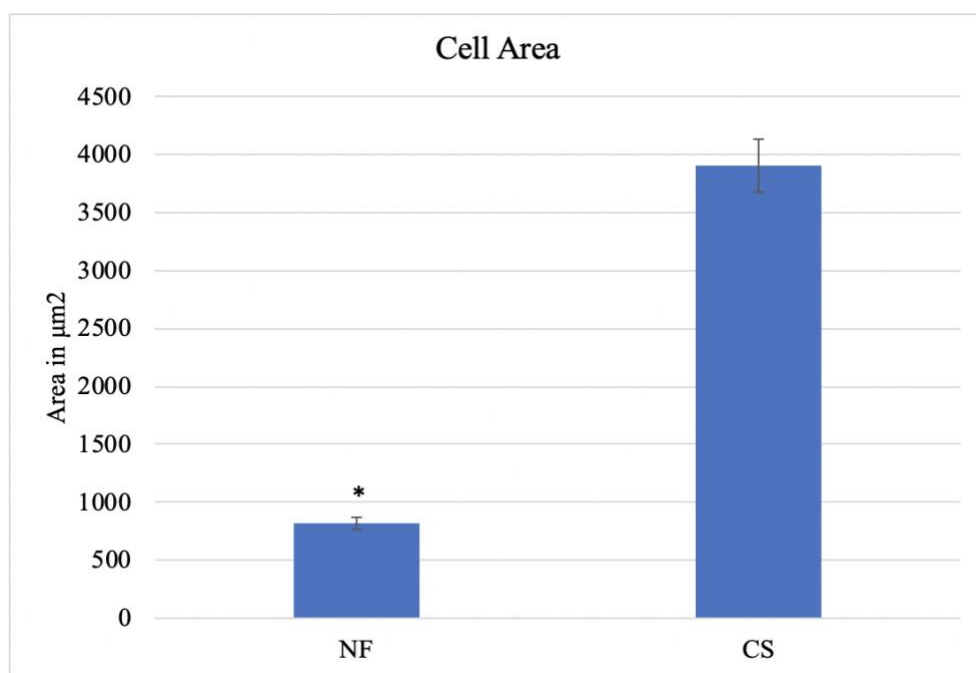


Figure 17: Average cell area of hMSCs seeded on 10% PMMA nanofibers or a PMMA control flat surface. * indicates $p < 0.05$ compared to control.

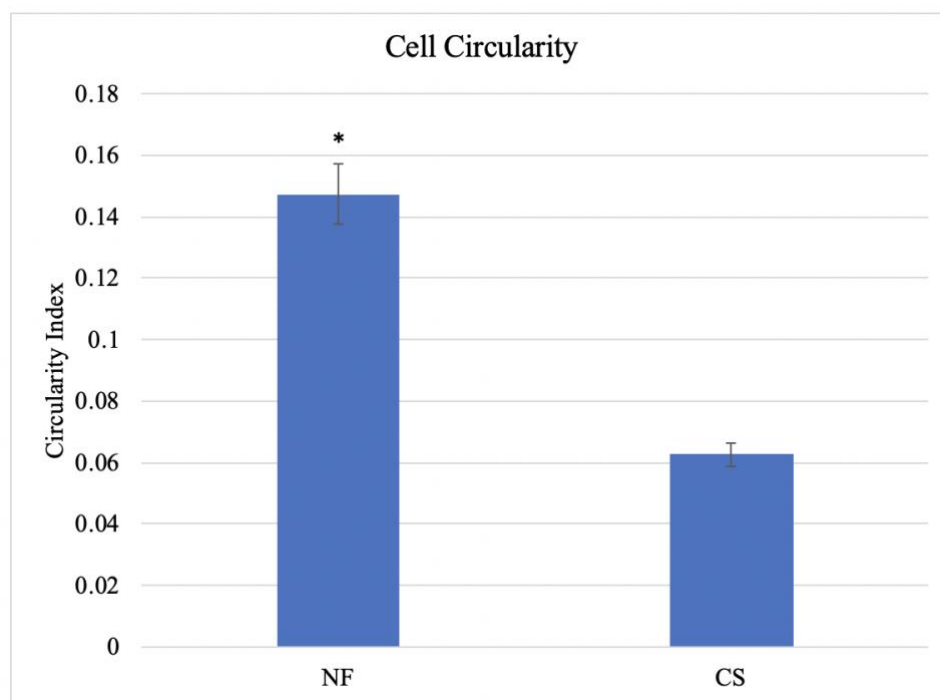


Figure 18: Average cell circularity of hMSCs seeded on 10% PMMA nanofibers or a PMMA control flat surface. * indicates $p < 0.05$ compared to control.

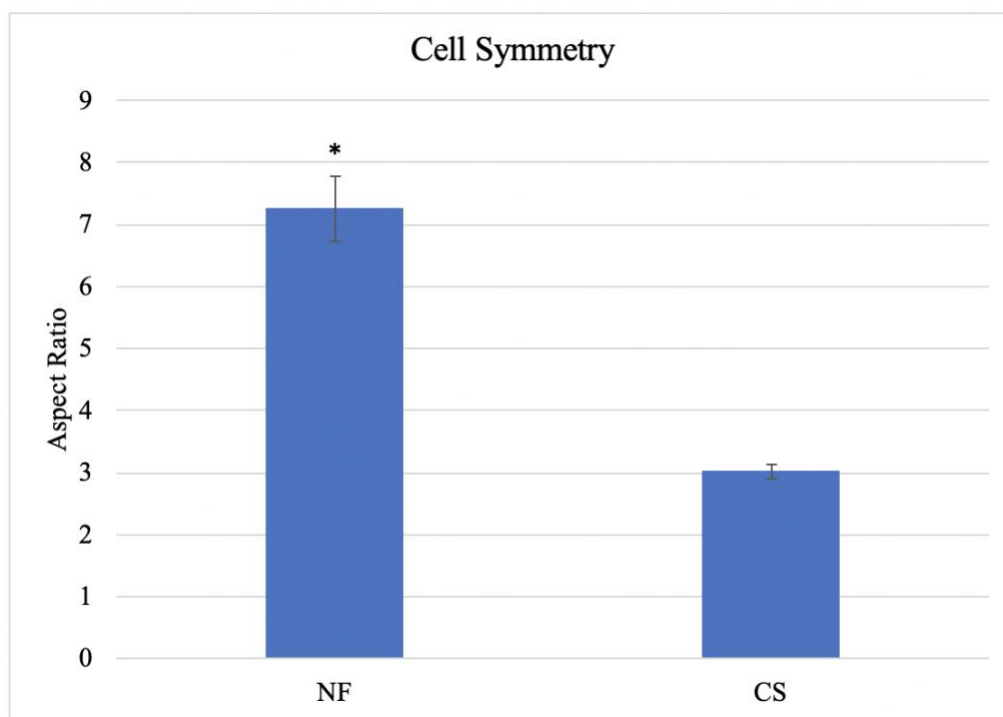


Figure 19: Average cell symmetry of hMSCs seeded on 10% PMMA nanofibers or a PMMA control flat surface. * indicates $p < 0.05$ compared to control.

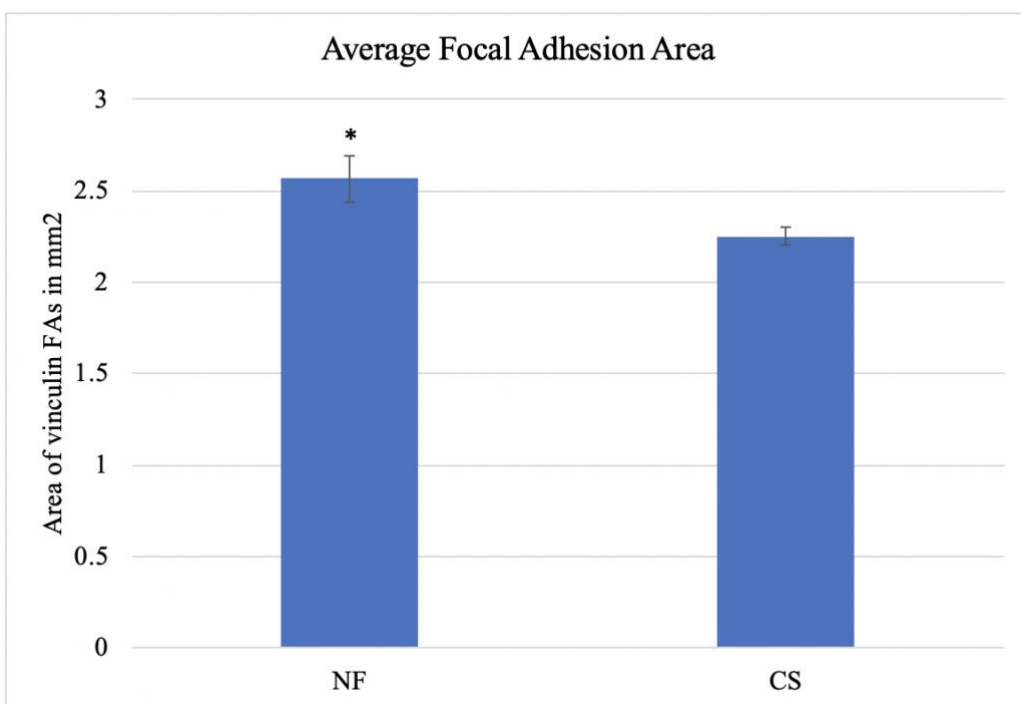


Figure 20: Average focal adhesion area of hMSCs seeded on 10% PMMA nanofibers or a PMMA control flat surface.

In this experiment, human MSCs were seeded onto glass coverslips at a density of 5,000 cells / cm². Cells were fixed after 24 hours and stained for vinculin, beta-5-integrin (both markers of focal adhesions), actin, and nuclei. Similar to experiment 1, cell area (816.76 vs 3904.01 vs μm^2) was lesser in cells grown on nanofiber surfaces, and symmetry (7.25 vs 3.02) was greater as compared to control. However, in this experiment, cell circularity (0.15 vs 0.06) was greater in nanofiber cells as compared to cells grown on control surfaces. This could potentially be explained by increased cell spreading or proliferation on the nanofiber surfaces. Moreover, ImageJ software was used to count focal adhesion area by quantifying the vinculin patches, and it was found that on average, cells grown on nanofiber surfaces have a greater focal adhesion area than controls (2.56 vs 2.25). This data supports the hypothesis that nanofiber surfaces promote the growth of cells in an in-vivo format through production of greater focal adhesions and may be better than control surfaces for inducing osteogenic differentiation.

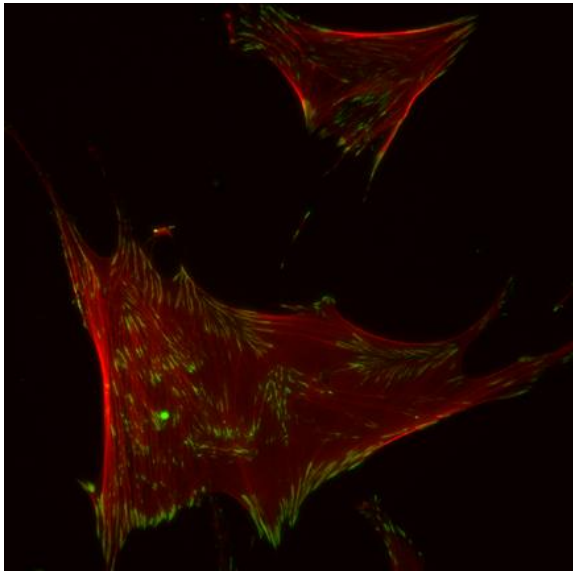


Figure 21: Vinculin staining (green) of hMSC on PMMA control surface

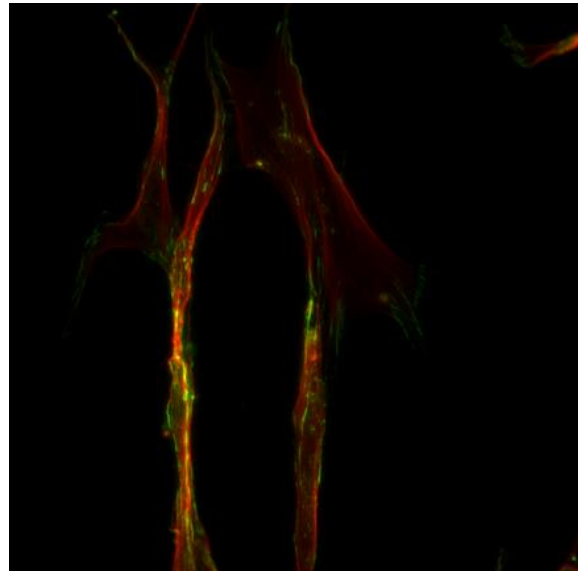


Figure 22: Vinculin staining (green) of hMSC on 10% PMMA Nanofiber

Experiment 3 – Nuclear YAP1 Localization on Small, Medium, and Large Fibers

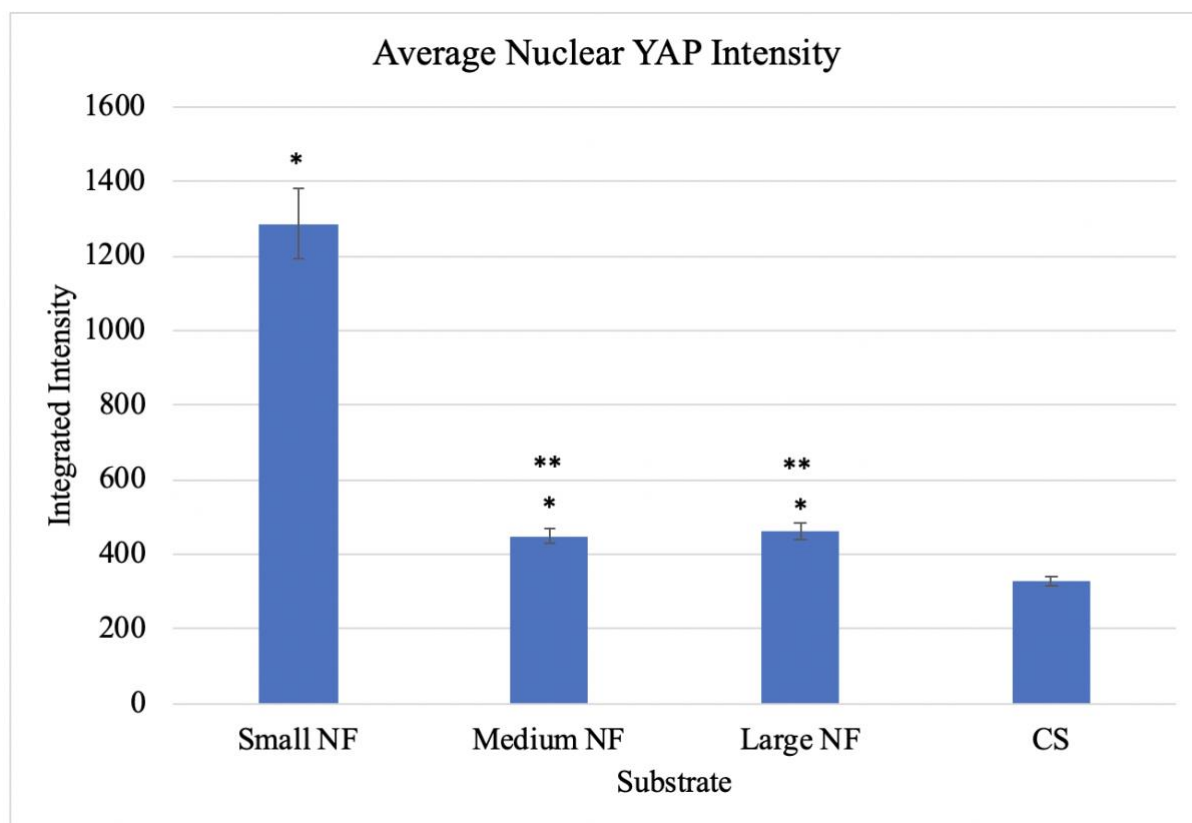


Figure 23: Average nuclear YAP1 fluorescence intensity of hMSCs seeded on 3%, 6.5%, or 10% nanofibers or a PMMA control flat surface. * indicates $p < 0.05$ compared to control. ** indicates $p < 0.05$ compared to 3% nanofibers.

Data from experiment 3 reveal that smaller nanofibers promote an increase in nuclear YAP1 localization. Cells were seeded, fixed, and stained with YAP1 in the same manner as experiments 1 and 2. Both medium (6.5%) and large (10%) nanofibers had a significantly greater amount of nuclear YAP1 intensity than cells grown on control PMMA surfaces (447.18 and 462.68 as compared to 326.75 respectively). However, cells grown on small nanofibers (3%) had a significantly greater amount of nuclear YAP1 localization (1286.86) than both the control surfaces and the medium and large nanofibers. These data provide evidence that smaller nanofibers may better mimic the extracellular microenvironment, promoting movement of YAP1

to the nucleus through colocalization with runx2, in turn promoting osteogenic differentiation. This knowledge allows for the better design and production of potential scaffold for biological generation of tissues, suggesting that growing cells on smaller nanofibers may promote bone growth.

ALP Experiments

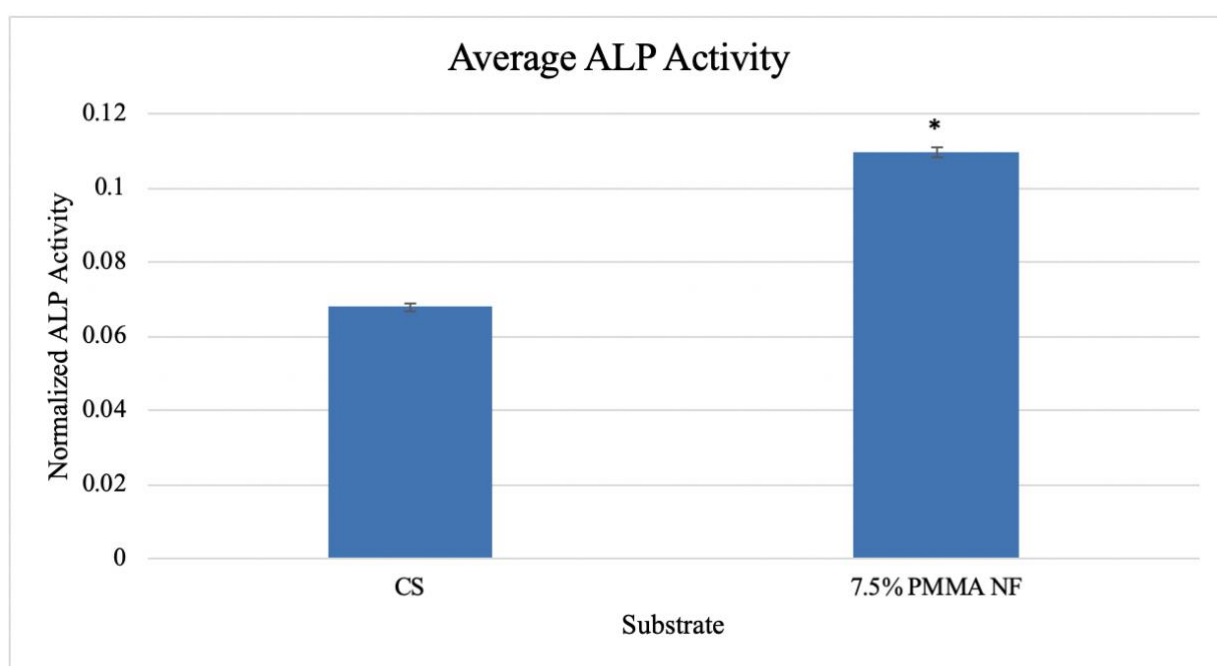


Figure 24: ALP activity of hMSCs seeded on 7.5% PMMA nanofibers or a PMMA control flat surface and incubated for 48 hours. * indicates $p < 0.05$ compared to control

In this experiment, detection of alkaline phosphatase (ALP) was used as a marker for osteogenic differentiation in hMSCs grown on both control and nanofiber surfaces. Cells were seeded onto surfaces at a density of 10,000 cells/cm² and grown for 1 week in differentiation medium. The cells were then lysed and transferred to a 96 well plate where ALP levels were detected. When normalized according to relative DNA levels using the pico green DNA assay, it

was found that cells grown on medium (7.5%) nanofibers show greater levels of osteogenic differentiation than those grown on flat PMMA control surfaces (0.110 vs. 0.068 respectively). These results support the evidence that nanofiber surfaces promote focal adhesion formation and nuclear YAP1 localization, leading to increased osteogenic differentiation.

In Cell Western Experiments

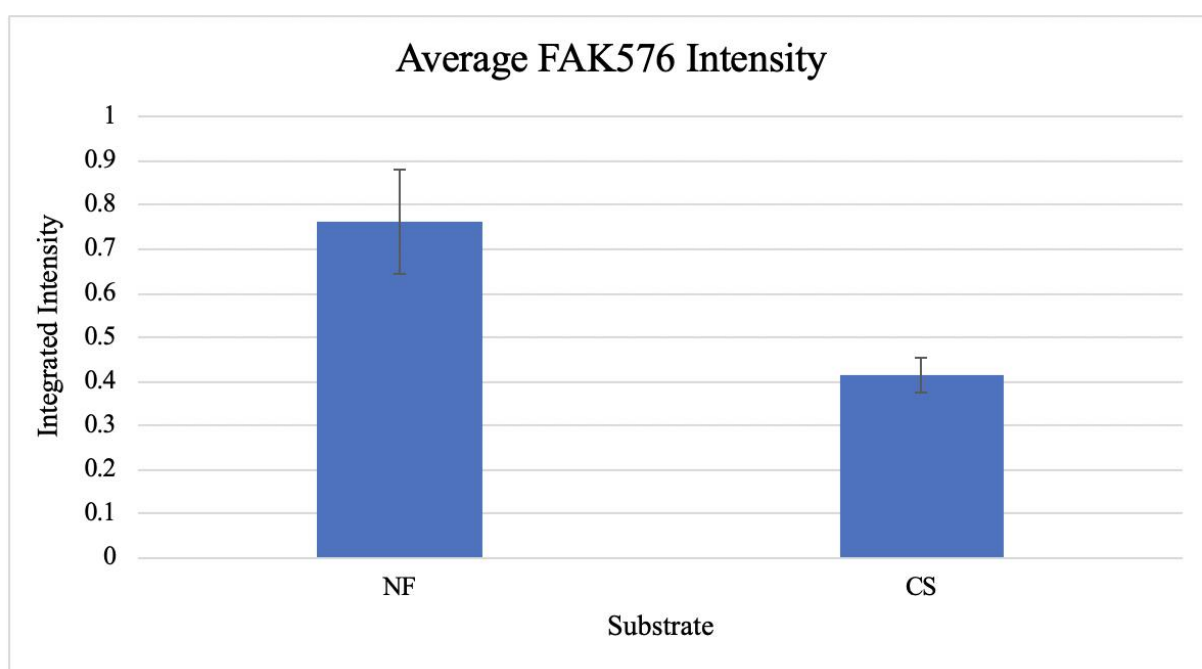


Figure 25: Average integrated FAK576 intensity of hMSCs seeded on 7.5% PMMA nanofibers or a PMMA control flat surface as indicated by in-cell western blot. n=2.

The next step in confirming the role of nanofiber surfaces in the FAK/RhoA/YAP1 pathway was to investigate FAK phosphorylation in response to varying substrate architecture. Cells were seeded onto medium (7.5%) nanofiber and control surfaces at a density of 10,000 cells/cm² and were stained with the FAK576 antibody as well as a cell tag stain to normalize expression levels. However, the results conflicted the hypothesis, showing increased FAK576

expression levels on nanofiber surfaces as compared to controls (average of 0.762 and 0.413 respectively). These results suggest a different function of FAK in FAK/RhoA/YAP1 pathway as previously thought and necessitate further experimentation about the role of FAK and its function in the promotion of osteogenic differentiation.

Chapter 4

Discussion / Future Work

Ultimately, it can be concluded that nanofiber surfaces as compared to flat controls promote osteogenic differentiation through the FAK/RhoA/YAP1 pathway, but the precise mechanism is still unclear. Decreased cellular confluency and a smaller nanofiber surface promote the nuclear localization of YAP1, providing evidence that YAP1 localization is regulated by means of cell-cell contacts rather than a temporal mechanism. Additionally, the nanofiber surface promotes an in-vivo like growth of the cell with a decreased area and increased symmetry, most likely due to even spreading on the fibers. However, results regarding cell circularity in response to local architecture are inconclusive. Moreover, a nanofiber surface increases focal adhesion area and concentration as well as osteogenic differentiation as shown through vinculin and alkaline phosphatase intensity respectively. This data supports the hypothesis that nanofiber surfaces increase focal adhesion formation and thus promote nuclear YAP1 localization and in turn osteogenesis.

On the other hand, results with respect to FAK phosphorylation do not coincide with the hypothesis, showing that nanofiber surfaces actually increase the phosphorylation of FAK at site 576. These results suggest a different function of FAK in the FAK/RhoA/YAP1 pathway as previously thought and necessitate further experimentation about the role of FAK and its function in the promotion of osteogenic differentiation.

Future work involves investigating this pathway further, specifically the role of FAK as it relates to osteogenesis. I propose staining for FAK and YAP1 with a ROCK inhibitor to see if ROCK inhibition has any downstream effects on localization of expression of other pathway

effectors. Additionally, staining for Runx2 in tandem with YAP may be helpful, as it is believed that YAP participates as a coactivator with Runx2 which promotes osteogenic differentiation. Ultimately, understanding the FAK/RhoA/YAP1 pathway through modification of substrate architecture may aid in the development of biomaterials for tissue regeneration and lay the foundation for the creation of a novel nanofibrous material.

Appendix A

Supplemental Information

Table 1: Average Proportion of YAP1 Negative Nuclei at Different Time Points

Time Point	Total Nuclei	Total Negative Nuclei	Percent	Average	Standard Deviation
24 hours	754	514	68.17	65.21	17.68
72 hours	2222	2108	94.87	94.21	4.43
1 week	1396	1331	95.34	96.8	3.42

Table 2: P-Values for Time Course Experiment

Data	P-Value
24 hours vs 72 hours	0.000493559
24 hours vs 1 week	0.000275974
72 hours vs 1 week	0.161459383

Table 3: Average Area, Aspect Ratio, Circularity Index, and Nuclear YAP1 Intensity of hMSCs seeded on 10% PMMA Nanofibers and Control Surfaces

Data Analyzed	10% PMMA NF	Control Slide
Average Area in μm^2	1407.11	3004.48
Standard Error	125.09	298.99
Average Aspect Ratio	5.45	2.24
Standard Error	0.34	0.13
Average Circularity Index	0.11	0.17
Standard Error	0.01	0.03
Average nuclear YAP1 intensity	274.12	186.71
Standard Error	15.19	8.56

Table 4: P-Values for Nanofiber Experiment 1

Data	P-Value
Area	1.91E-06
Aspect Ratio	7.20E-17
Circularity Index	0.04661313
Nuclear YAP1 Intensity	1.02E-06

Table 5: Average Area, Aspect Ratio, Circularity Index, and Vinculin Patch Area of hMSCs seeded on 10% PMMA Nanofibers and Control Surfaces

Data Analyzed	10% PMMA NF	Control Slide
Average Area in μm^2	816.76	3904.01
Standard Error	49.63	230.49
Average Aspect Ratio	7.25	3.02
Standard Error	0.51	0.12
Average Circularity Index	0.15	0.06
Standard Error	0.01	0
Average vinculin patch area in μm^2	2.56	2.25
Standard Error	0.13	0.05

Table 6: P-Values for Nanofiber Experiment 2

Data	P-Value
Area	1.52E-29
Aspect Ratio	5.34E-14
Circularity Index	4.91E-14
Average Vinculin Patch Area	1.56E-25

Table 7: Average Nuclear YAP1 Intensity of hMSCs seeded on 3,6.5, or 10% PMMA Nanofibers or a Flat Control Surface

Data Analyzed	CS	3% PMMA NF	6.5% PMMA NF	10% PMMA NF
Average nuclear YAP1 intensity	326.75	1286.86	447.18	462.98
Standard Error	12.16	93.51	20.75	22.38

Table 8: P-Values for Nanofiber Experiment 3

Data	P-value
CS vs 3% PMMA NF	3.32E-18
CS vs 6.5% PMMA NF	1.40E-06
CS vs 10% PMMA NF	5.57E-07
3% PMMA NF vs 6.5% PMMA NF	6.60E-15
3% PMMA NF vs 10% PMMA NF	1.89E-14
6.5% PMMA NF vs 10% PMMA NF	0.60547454

Table 9: Average ALP Intensity of hMSCs grown on 7.5% PMMA Nanofibers or Flat Control Surfaces

Data Analyzed	7.5% PMMA Nanofiber	Control Surface
Average	0.10982088	0.067882336
Standard Error	0.00145121	0.001179327
P-Value	0.001048041	

Table 10: Average Intensity of FAK576 of hMSCs Seeded on 7.5% PMMA Nanofibers of Flat Control Surfaces

Data Analyzed	7.5% PMMA Nanofiber	Control Surface
Average Intensity	0.762490203	0.412933792
Standard Deviation	0.239923945	0.077834214
Standard Error	0.119961973	0.038917107
P-Value	0.056116636	

BIBLIOGRAPHY

1. Amini, A. R., Laurencin, C. T., & Nukavarapu, S. P. (2012). Bone tissue engineering: recent advances and challenges. *Critical Reviews™ in Biomedical Engineering*, 40(5).
2. Jahangir, A. A., Nunley, R. M., Mehta, S., & Sharan, A. (2008). Bone-graft substitutes in orthopaedic surgery. *AAos now*, 2(1), 35-37.
3. Fernandez de Grado, G., Keller, L., Idoux-Gillet, Y., Wagner, Q., Musset, A. M., Benkirane-Jessel, N., ... & Offner, D. (2018). Bone substitutes: a review of their characteristics, clinical use, and perspectives for large bone defects management. *Journal of tissue engineering*, 9, 2041731418776819.
4. Laurencin, C. T., Ambrosio, A. M. A., Borden, M. D., & Cooper Jr, J. A. (1999). Tissue engineering: orthopedic applications. *Annual review of biomedical engineering*, 1(1), 19-46.
5. Dimitriou, R., Jones, E., McGonagle, D., & Giannoudis, P. V. (2011). Bone regeneration: current concepts and future directions. *BMC medicine*, 9(1), 66.
6. Einhorn, T. A. (1998). The cell and molecular biology of fracture healing. *Clinical Orthopaedics and Related Research®*, 355, S7-S21.
7. McKibbin, B. (1978). The biology of fracture healing in long bones. *The Journal of bone and joint surgery. British volume*, 60(2), 150-162.
8. Ridley, A. J., Schwartz, M. A., Burridge, K., Firtel, R. A., Ginsberg, M. H., Borisy, G., ... & Horwitz, A. R. (2003). Cell migration: integrating signals from front to back. *Science*, 302(5651), 1704-1709.

9. Panzetta, V., Fusco, S., & Netti, P. A. (2019). Cell mechanosensing is regulated by substrate strain energy rather than stiffness. *Proceedings of the National Academy of Sciences*, 201904660.
10. Ozdemir, T., Xu, L. C., Siedlecki, C., & Brown, J. L. (2013). Substrate curvature sensing through Myosin IIa upregulates early osteogenesis. *Integrative Biology*, 5(11), 1407-1416.
11. James, R., Toti, U. S., Laurencin, C. T., & Kumbar, S. G. (2011). Electrospun nanofibrous scaffolds for engineering soft connective tissues. In *Biomedical Nanotechnology* (pp. 243-258). Humana Press.
12. Hu, J., Liu, X., & Ma, P. X. (2008). Induction of osteoblast differentiation phenotype on poly (L-lactic acid) nanofibrous matrix. *Biomaterials*, 29(28), 3815-3821.
13. Chang, B., Ma, C., & Liu, X. (2018). Nanofibers regulate single bone marrow stem cell osteogenesis via FAK/RhoA/YAP1 pathway. *ACS applied materials & interfaces*, 10(39), 33022-33031.
14. Tomlinson, V., Gudmundsdottir, K., Luong, P., Leung, K. Y., Knebel, A., & Basu, S. (2010). JNK phosphorylates Yes-associated protein (YAP) to regulate apoptosis. *Cell death & disease*, 1(2), e29.
15. Kodaka, M., & Hata, Y. (2015). The mammalian Hippo pathway: regulation and function of YAP1 and TAZ. *Cellular and molecular life sciences*, 72(2), 285-306.
16. Low, B. C., Pan, C. Q., Shivashankar, G. V., Bershadsky, A., Sudol, M., & Sheetz, M. (2014). YAP/TAZ as mechanosensors and mechanotransducers in regulating organ size and tumor growth. *FEBS letters*, 588(16), 2663-2670.

17. Dupont, S., Morsut, L., Aragona, M., Enzo, E., Giulitti, S., Cordenonsi, M., ... & Elvassore, N. (2011). Role of YAP/TAZ in mechanotransduction. *Nature*, *474*(7350), 179.
18. Das, A., Fischer, R. S., Pan, D., & Waterman, C. M. (2016). YAP nuclear localization in the absence of cell-cell contact is mediated by a filamentous actin-dependent, myosin II- and phospho-YAP-independent pathway during extracellular matrix mechanosensing. *Journal of Biological Chemistry*, *291*(12), 6096-6110.
19. Schlaepfer, D. D., Hauck, C. R., & Sieg, D. J. (1999). Signaling through focal adhesion kinase. *Progress in biophysics and molecular biology*, *71*(3-4), 435-478.
20. Sieg, D. J., Hauck, C. R., Ilic, D., Klingbeil, C. K., Schaefer, E., Damsky, C. H., & Schlaepfer, D. D. (2000). FAK integrates growth-factor and integrin signals to promote cell migration. *Nature cell biology*, *2*(5), 249.
21. Nardone, G., Oliver-De La Cruz, J., Vrbsky, J., Martini, C., Pribyl, J., Skládal, P., ... & Maceckova, Z. (2017). YAP regulates cell mechanics by controlling focal adhesion assembly. *Nature communications*, *8*, 15321.
22. Watanabe, N., Kato, T., Fujita, A., Ishizaki, T., & Narumiya, S. (1999). Cooperation between mDial1 and ROCK in Rho-induced actin reorganization. *Nature cell biology*, *1*(3), 136.
23. Zhang, H., Cooper, L. F., Zhang, X., Zhang, Y., Deng, F., Song, J., & Yang, S. (2016). Titanium nanotubes induce osteogenic differentiation through the FAK/RhoA/YAP cascade. *RSC Advances*, *6*(50), 44062-44069.

ACADEMIC VITA

Anastasia Hale

Education:

High School Diploma / 2016 / Baldwin High School

Bachelor of Science / 2020 / The Pennsylvania State University

Major: Biology - Vertebrate Physiology Option

Minor: German

Schreyer Honors College

Millennium Scholars Program

Accepted to the MD/PhD Program at the Penn State College of Medicine for admission in 2020

Research Experience:

Musculoskeletal Regenerative Engineering Lab at Penn State **1/17- 5/20**

MD/PhD Summer Exposure Program in the Moldovan Lab at The Penn State College of Medicine **6/17-8/17, 6/18-8/18**

DAAD Rise Undergraduate Fellowship in the Nikolaus-Fiebiger Center for Molecular Medicine at Friedrich-Alexander Universität Erlangen-Nürnberg; Erlangen, Germany **5/19-8/19**

Honors and Awards:

Guglielmelli Honors Scholarship in Science 2016, 2017

McKinstry Scholarship 2016-2019

Burstein Memorial Scholarship in Science 2018

Travel Award from Southeastern Medical Scientist Symposium 2018

Third Place for Best Undergraduate/Post Bac Oral Presentation at the Southeastern Medical Scientist Symposium 2018

Eberly College of Science Undergraduate Science Engagement Research Funding Award 2018

Extracurricular Activities:

- Penn State University Biomedical Sciences Club
Social Chair (2016), Secretary (2017), Vice President (2018)
- Tutor for Biology 110 (2017) – Organized lesson plans and taught fundamental biology concepts to undergraduate students in the Millennium Scholars Program
- IES Abroad Student Ambassador (2018) – Connect students with IES Study Abroad opportunities and organize presentations and events on campus about international study experiences
- Volunteer as Penn State Study Abroad Peer Ambassador (2018) – Hold weekly office hours to connect students with study abroad opportunities and speak as a representative at study abroad events and involvement fairs

International Experience

- IES Vienna: European Society and Culture Program (2018) – Study abroad experience in Vienna, Austria taking an advanced German course load following a ‘German Intensive’ Period